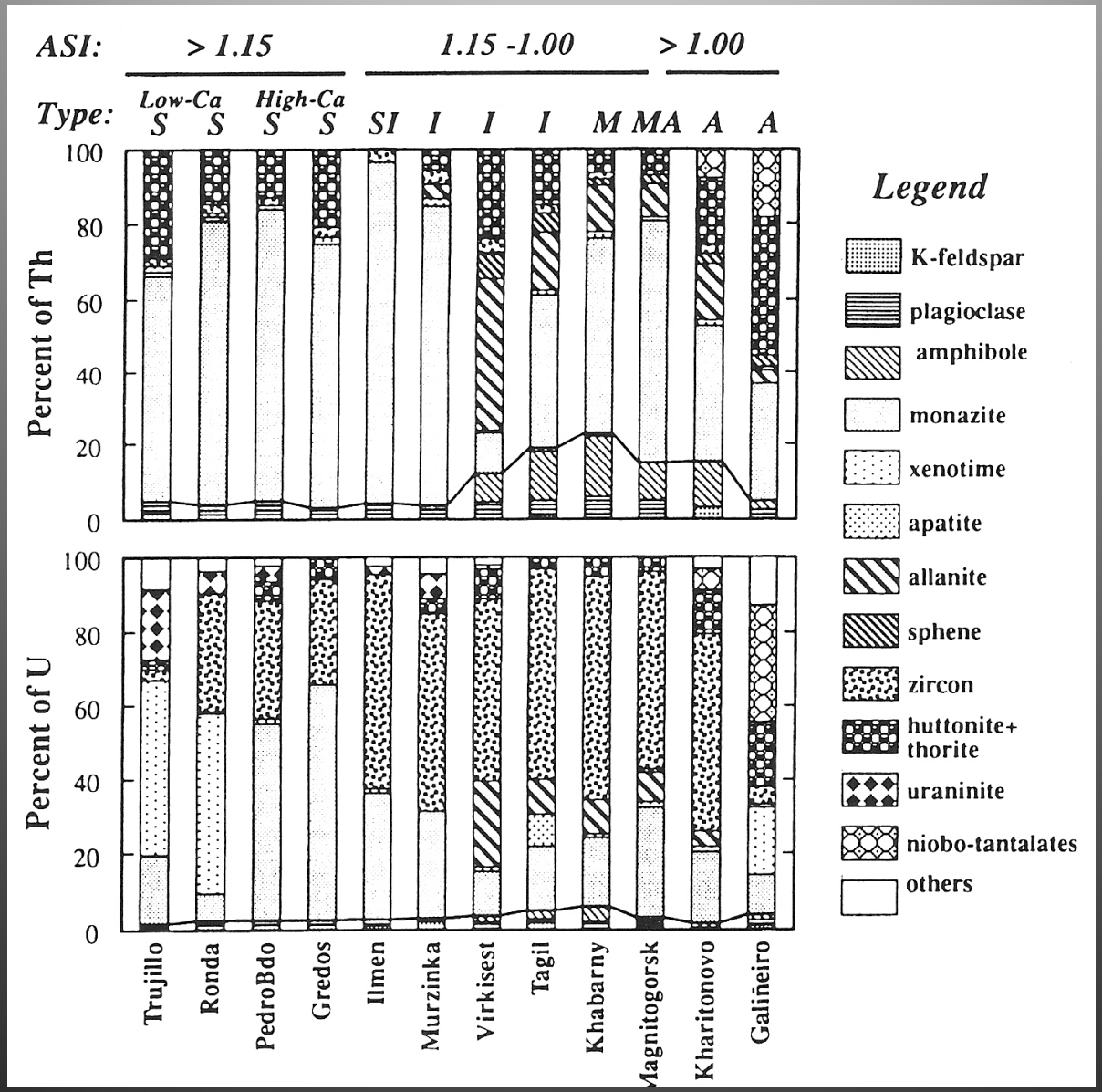

Bea F, 1996

Fig. 18. Fractional contribution of each mineral to the whole-rock Th and U budgets in selected granite plutons. Continuous line separates the contribution of major from accessory minerals. Dashed line separates the contribution of accessory phosphates from silicates. Dotted line separates accessory silicates from niobotantalates and carbonates. (See discussion in text.)

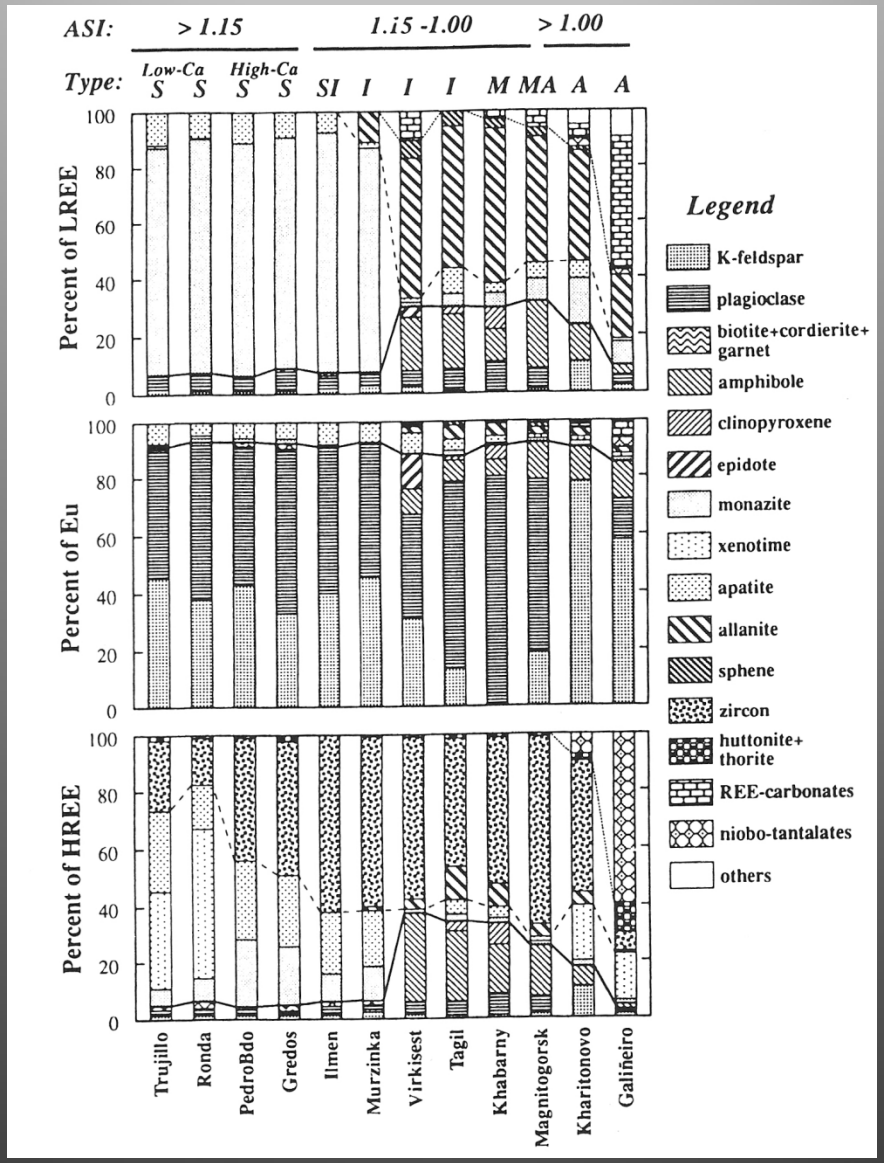

Bea F, 1996

Fig. 17. Fractional contribution of each mineral to the whole-rock LREE, Eu and HREE budgets in selected granite plutons. Continuous line separates the contribution of major from accessory minerals. Dashed line separates the contribution of accessory phosphates from silicates. Dotted line separates accessory silicates from niobotantalates and carbonates. (See discussion in text.)

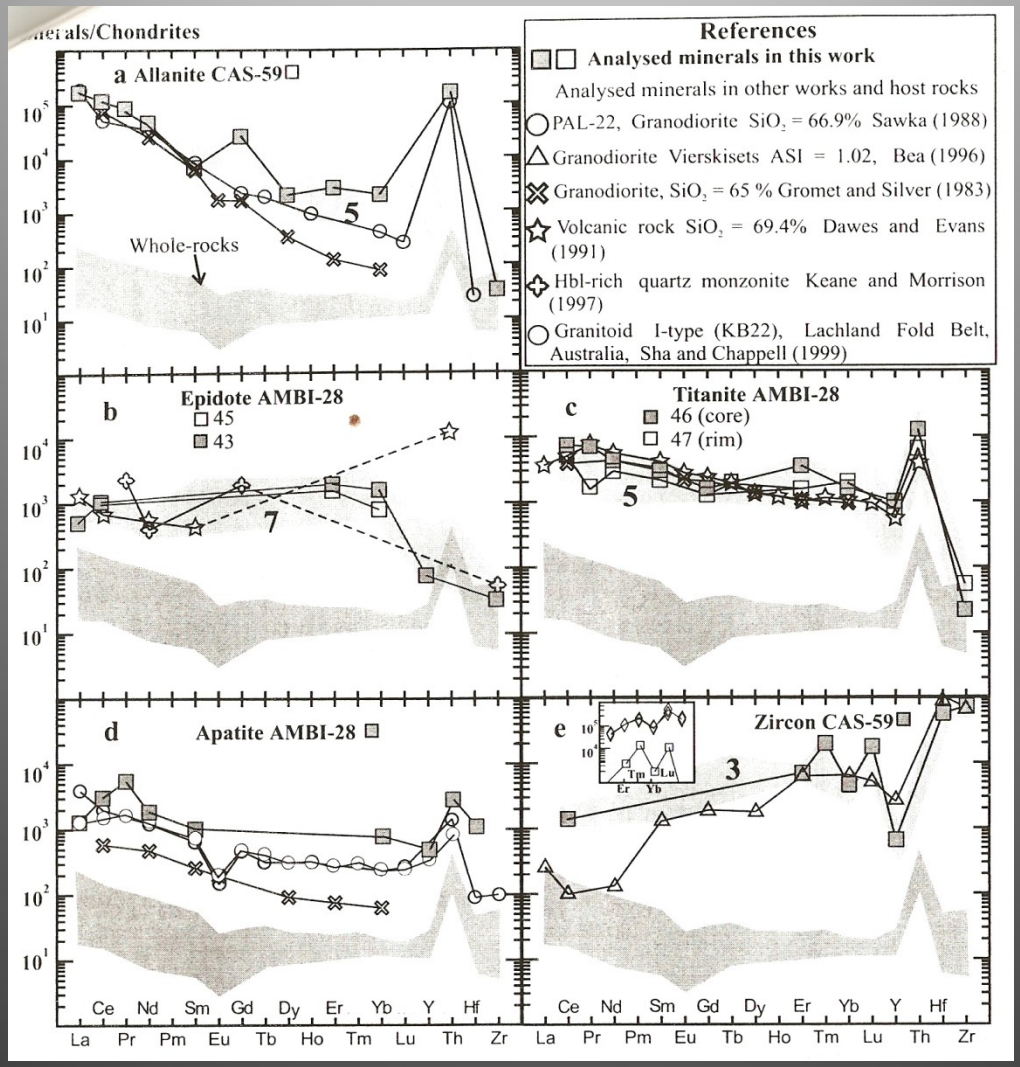

Dahlquist JA, 2001

FIG. 2. Chondrite-normalized trace element patterns of minerals analysed in this and other works. Normalized values for *REE* after Nakamura (1974) and for Y, Th, Hf and Zr after Thompson (1982). The lower shaded fields represent the whole-rock trace element chondrite-normalized patterns for the granitic rocks of the Sierra de Chepes (see details in Fig. 3). The upper shaded fields represent the mineral trace element chondrite-normalized patterns for allanite, epidote, titanite, apatite and zircon. The numbers over the shaded fields indicate the number of analyses. Apatite has only one analysis. (*e*) The Tm and Lu contents in xenotime, determined by González del Tánago (1997) (diamond symbol), are compared with the Tm and Lu contents in zircon.

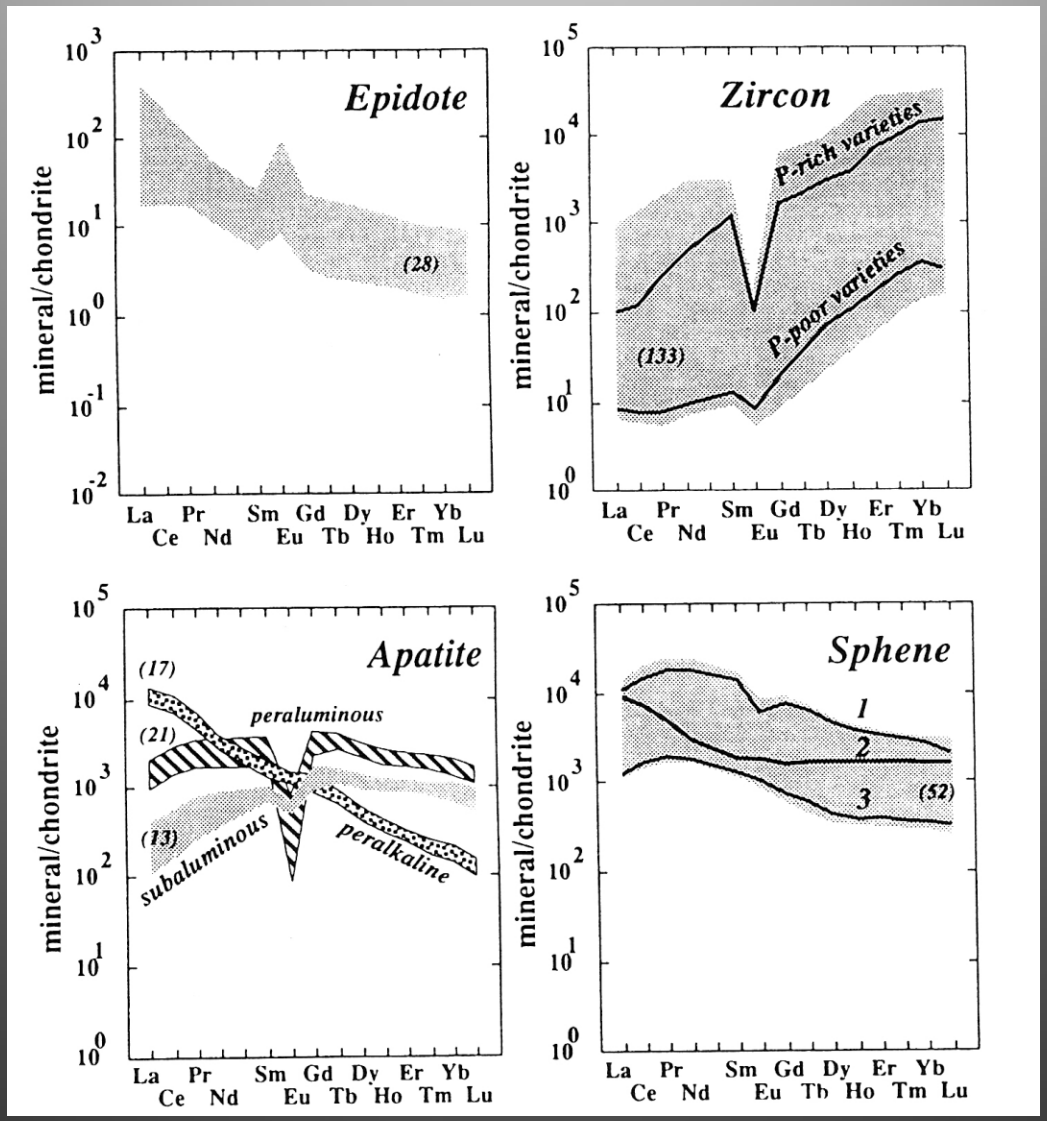

Bea F, 1996

Fig. 4. Chondrite-normalized REE patterns of epidote, zircon, apatite and sphene. Shaded areas represent fields occupied by analysed specimens; the number of analyses represented is shown in parentheses. For sphene, 1 and 3 represent extreme cases of sphenes from metaluminous granitoids (note the decreased intensity of the Eu anomaly as ΣREE decreases; 2 represents the characteristic pattern of sphenes from peralkaline granites.

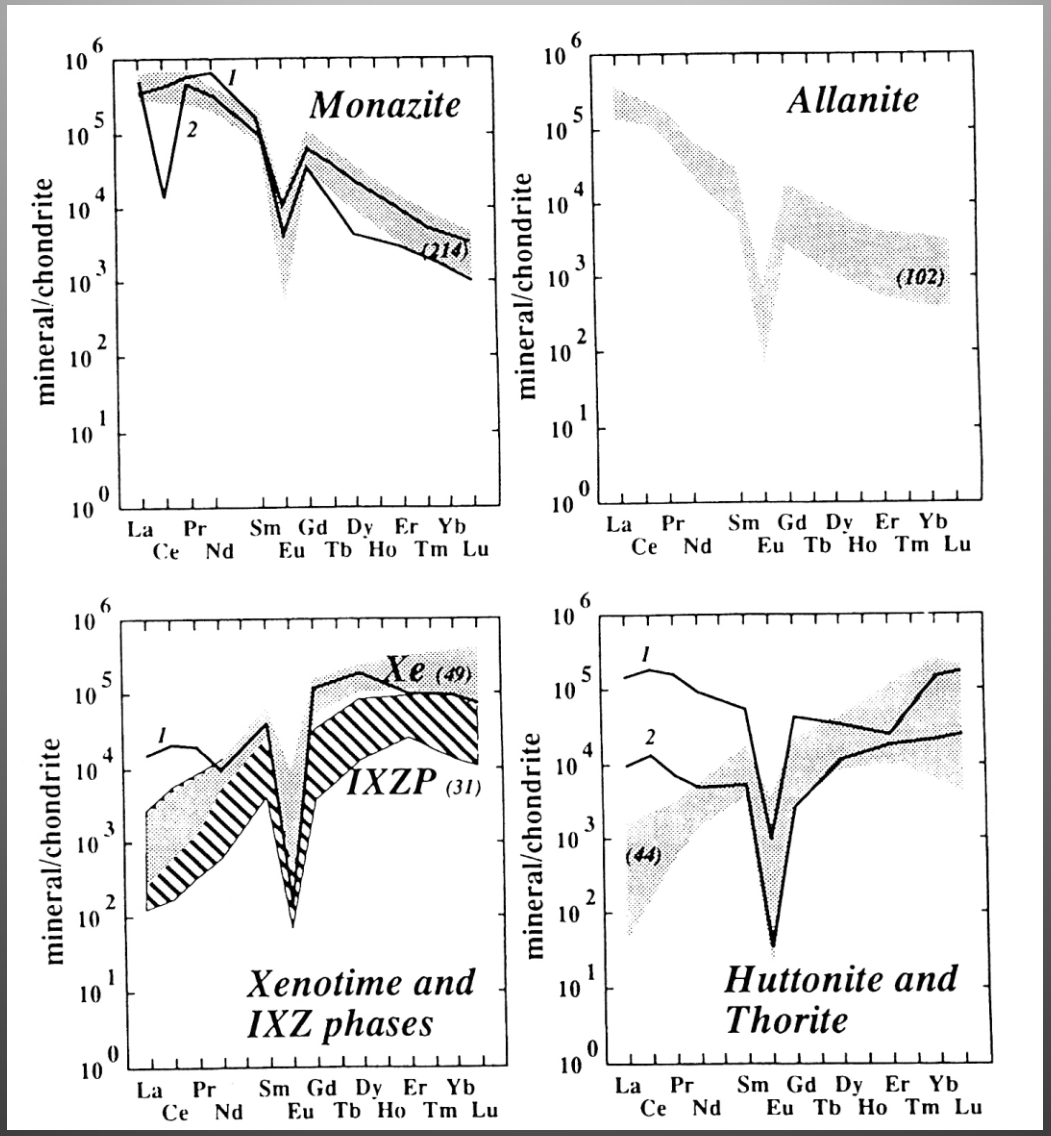

Bea F, 1996

Fig. 8. Chondrite-normalized REE patterns of monazite, allanite, xenotime, intermediate xenotime–zircon phases (IXZP) and Th-orthosilicate minerals. Shaded areas represent fields occupied by analysed specimens; the number of analyses represented is shown in parentheses. Monazite: 1, Nd-rich variety; 2, Ce-depleted monazite associated with secondary cerianite (see text). Xenotime: 1, intermediate xenotime–monazite phase. Th-orthosilicates: 1 and 2, LREE- and P-rich varieties, probably monazite–huttonite solid solution phases.

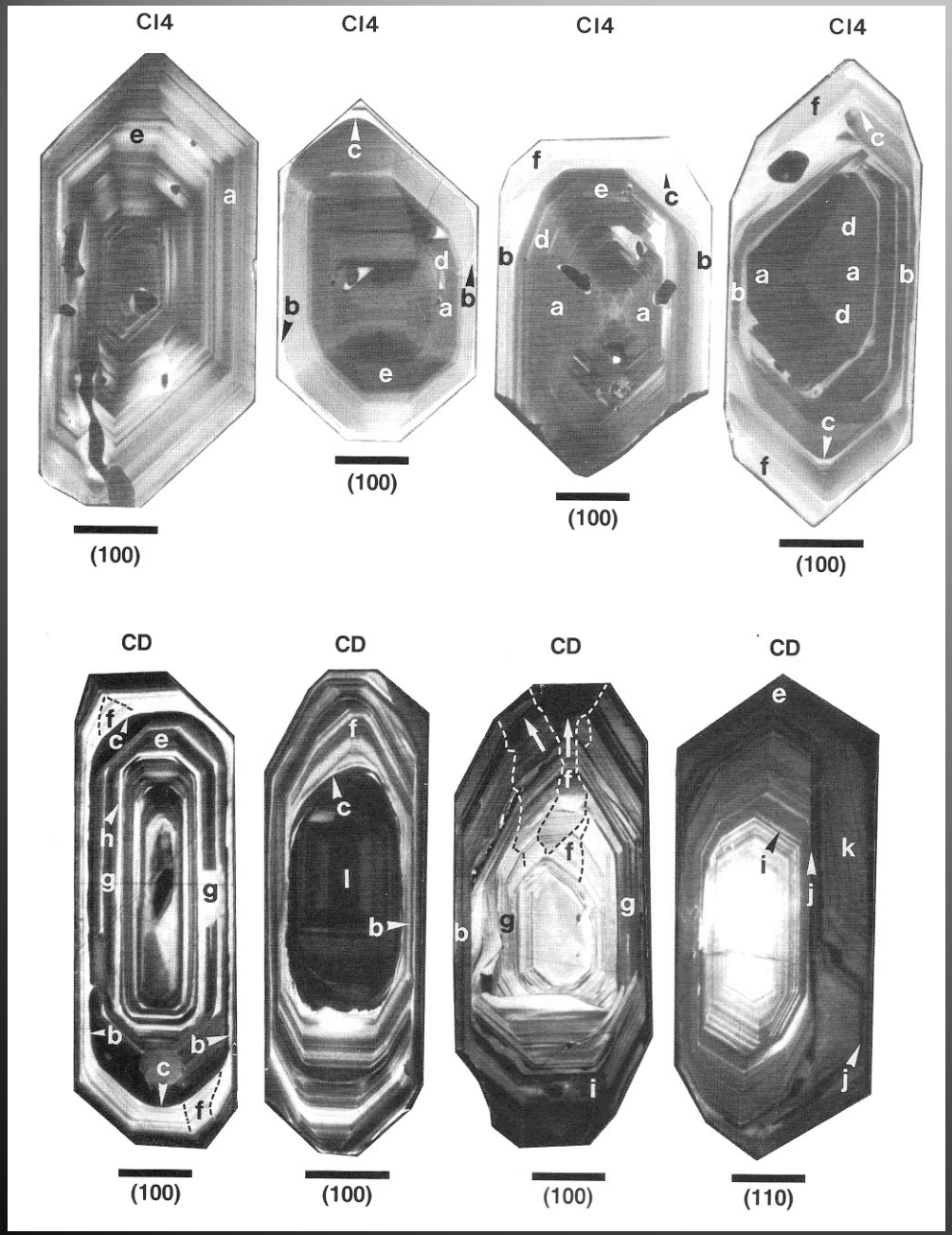

Fig. 4 Cathodoluminescence images of zircon sections. *CI4*, from alkaline granitoids of the Monte Cinto ring complex, *CD*, from high-K calcalkaline granodiorite of Cima d'Asta. *a*, rapid growth of {010} relative to pyramidal faces; *b*, strongly reduced growth rate of {010}; *c*, stages of crystal corrosion overgrown by brightly luminescent bands; *d*, presence of {031} during rapid growth of {010}; *e*, symmetric growth of {011}; *f*, asymmetric growth of {011} (the typical irregular shape of sector boundaries is marked by *dashed lines*); *g*, irregularly fluctuating growth rate of {010}; *h*, intercalated brightly luminescent growth bands; *i*, continuous transition to low-luminescent outer growth zone; *j*, growth inhibition of (110); *k*, resumption of rapid growth on (110) by curved growth bands; *l*, possible inherited core. *Scale bars* 30 µm. The indices below denote the section planes

Vavra G, 1994

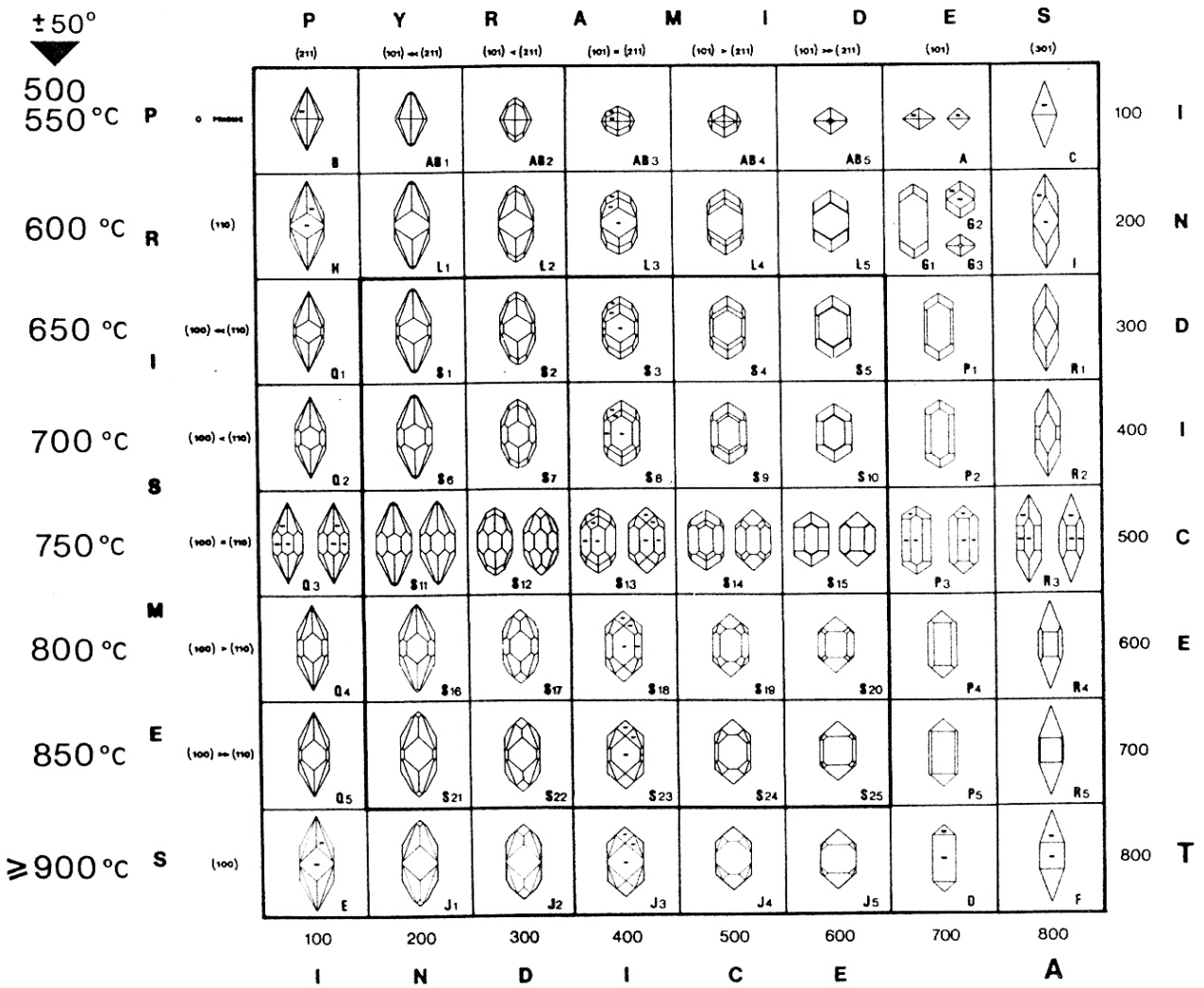

Fig. 1 Main types and subtypes of the typologic classification and corresponding geothermometric scale. The two variables (A, T) depend upon the relative development of the crystalline faces (respectively pyramids and prisms of the zircon).

Pupin JP, 1985

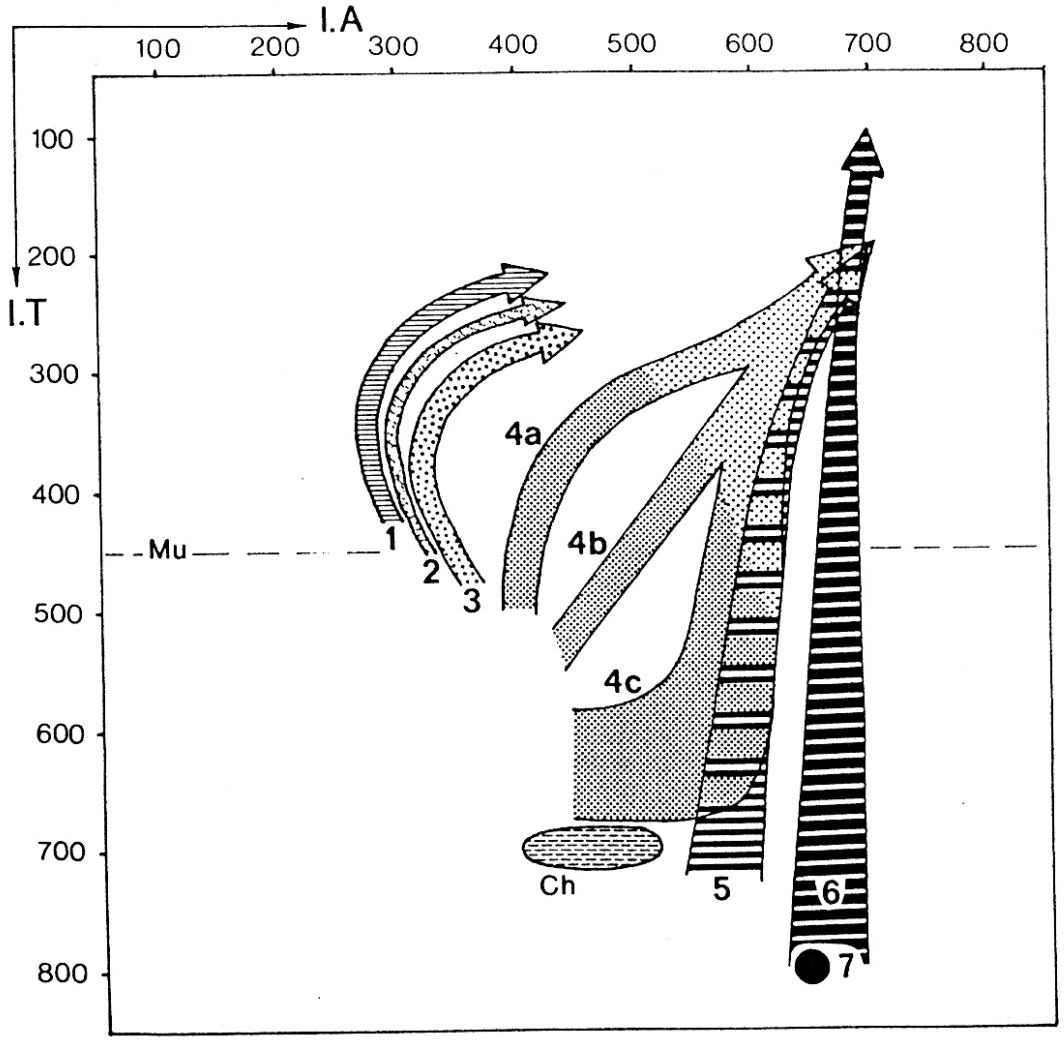

Fig. 2 Distribution of mean points and mean Typological Evolutionary Trends of zircon populations (PUPIN, 1980) from: Aluminous anatectic granites: (1) aluminous leucogranites; (2) (par)autochthonous monzogranites and granodiorites; (3) intrusive aluminous monzogranites and granodiorites. – Hybrid granites of crustal + mantle origin: (4 a, b, c) calc-alkaline series granites *(dark doted area* = granodiorites + monzogranites; *clear doted area* = monzogranites + alkaline granites); (5) sub-alkaline series granites. – Granites of mantle or mainly mantle origin: (6) alkaline series granites; (7) tholeiitic series granites. – *Mu*, limit of the muscovite granites (I.T < 450); *Ch*, magmatic charnockites area.

Pupin JP, 1985

Abstract. Based on microprobe work, we present arguments that the size relations of the two common prisms {100} and {110} of accessory granite zircons are strongly influenced by chemical factors. Magmatic growth zoning patterns, which we have studied by means of backscattered electron imaging in special zircon sections orientated perpendicular to the c-axis, do not support previous models which assumed temperature or the degree of $ZrSiO_4$ supersaturation to be the primary prism-form-directing factors. The element U, which usually occupies the Zr-sites of granite zircons to some degree, is strongly suspected of producing an (adsorptive) growth-blocking effect for {110}-type faces thus creating crystals with {110}-dominated prism morphology. A second independent mechanism that is likely to form zircons with large {110} prisms is the common substitution $Zr^{4+} + Si^{4+}$ versus $Y(REE)^{3+} + P^{5+}$. Granitic melts with low U (Th), Y(REE) and P contents (relative to Zr) are, according to our model, predestinated to produce zircons with large {100} prisms and vice versa.

Benisek A, Finger F, 1993

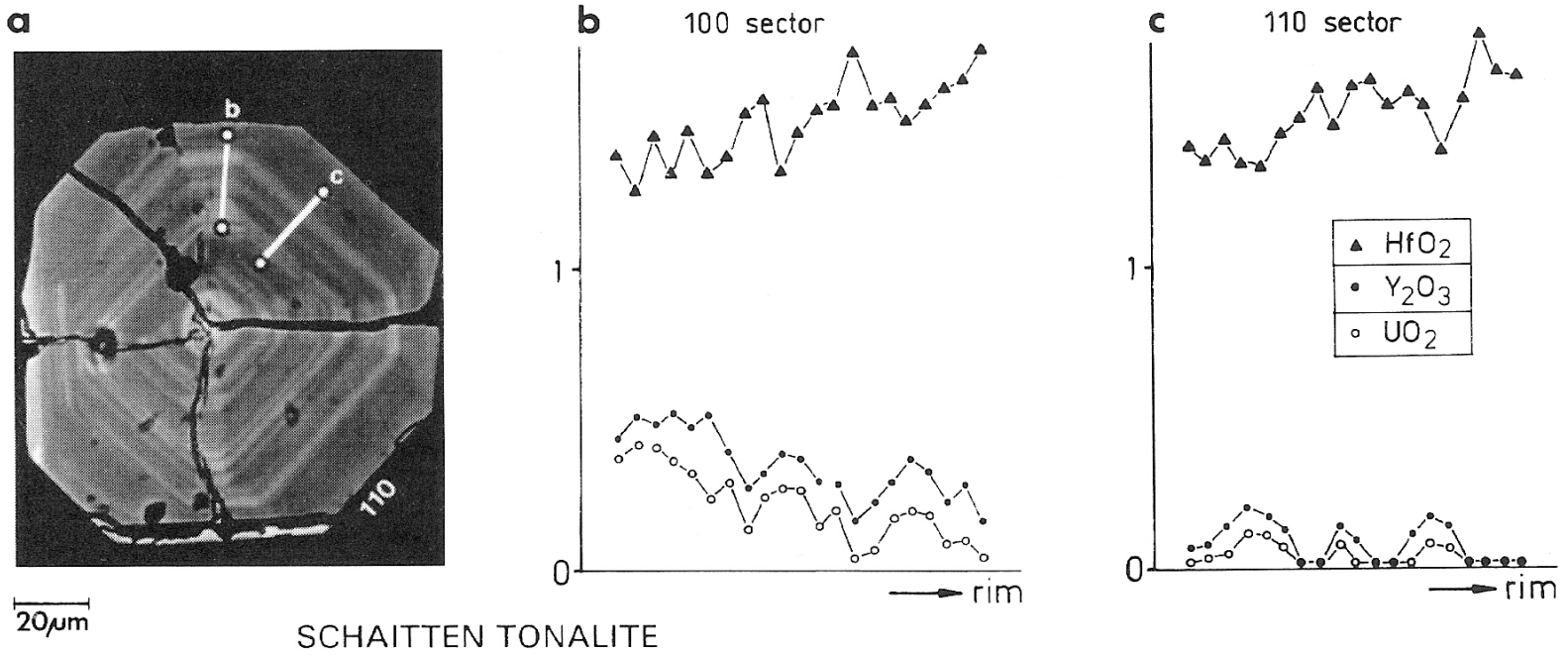

Fig. 2. Typical example of oscillatory growth zoning of prism faces in zircon (a) (orientation of section is perpendicular to the c-axis – see Fig. 1). The particular magmatic zoning patterns of the grain are discussed in detail in the text. The effect of {100} versus {110} sector zoning is demonstrated in the chemical profiles in (**b**) and (**c**) (concentrations are always in wt% oxides; Th, HREE and P are mostly at or below detection limit in both traverses and not shown). In the centre of the grain is a small rounded and probably inherited core that is relatively rich in UO_2 (ca. 0.5 wt%), Y_2O_3 (ca. 0.8 wt%), Yb_2O_3 (ca. 0.2 wt%) and P_2O_5 (ca. 0.8 wt%)

Benisek A, Finger F, 1993